Research article

Structural, Functional and Clinical Characterization of a Novel *PTPN11* Mutation Cluster Underlying Noonan Syndrome

Running Title: Novel *PTPN11* mutation cluster in Noonan syndrome

Luca Pannone[1,2,3], Gianfranco Bocchinfuso[4], Elisabetta Flex[2], Cesare Rossi[5], Giuseppina Baldassarre[6], Christina Lissewski[7], Francesca Pantaleoni[1], Federica Consoli[8], Francesca Lepri[1], Monia Magliozzi[1,8], Massimiliano Anselmi[4], Giovanni Sorge[9], Kadri Karaer[10], Goran Cuturilo[11,12], Alessandro Sartorio[13,14], Sigrid Tinschert[15], Maria Accadia[8], Maria C. Digilio[1], Giuseppe Zampino[16], Alessandro De Luca[8], Hélène Cavé[17,18], Martin Zenker[7], Bruce D. Gelb[19], Bruno Dallapiccola[1], Lorenzo Stella[4], Giovanni B. Ferrero[6], Simone Martinelli[2¶*], Marco Tartaglia[1¶*]

[1]Genetics and Rare Diseases Research Division, Ospedale Pediatrico Bambino Gesù, IRCCS, Rome, Italy. [2]Dipartimento di Ematologia, Oncologia e Medicina Molecolare, Istituto Superiore di Sanità, Rome, Italy. [3]Dipartimento di Medicina Sperimentale, Sapienza Università di Roma, Rome, Italy. [4]Dipartimento di Scienze e Tecnologie Chimiche, Università di Roma Tor Vergata, Rome, Italy. [5]Genetica Medica, Policlinico S. Orsola-Malpighi, Bologna, Italy. [6]Department of Pediatric and Public Health Sciences, University of Torino, Torino, Italy. [7]Institute of Human Genetics, University Hospital of Magdeburg, Otto-von-Guericke-University, Magdeburg, Germany. [8]Ospedale Casa Sollievo della Sofferenza,

This article has been accepted for publication and undergone full peer review but has not been through the copyediting, typesetting, pagination and proofreading process, which may lead to differences between this version and the Version of Record. Please cite this article as doi: 10.1002/humu.23175.

IRCCS, San Giovanni Rotondo, Italy. [9]Unità Operativa Complessa di Clinica Pediatrica, Dipartimento di Medicina Clinica e Sperimentale, Università di Catania, Catania, Italy. [10]Dr. Ersin Arslan Research and Training Hospital, Department of Medical Genetics, Gaziantep, Turkey. [11]Faculty of Medicine, University of Belgrade, Belgrade, Serbia. [12]University Children's Hospital, Belgrade, Serbia. [13]Istituto Auxologico Italiano, Experimental Laboratory for Auxo-Endocrinological Research, Milan and Verbania, Italy. [14]Istituto Auxologico Italiano, Division of Auxology, Verbania, Italy. [15]Institute of Clinical Genetics, Technical University of Dresden, Dresden, Germany. [16]Istituto di Clinica Pediatrica, Università Cattolica del Sacro Cuore, Rome, Italy. [17]Département de Génétique, Hôpital Robert Debré, Paris, 75019, France. [18]INSERM UMR_S1131, Institut Universitaire d'Hématologie, Université Paris Diderot, Paris-Sorbonne-Cité, Paris, 75205, France. [19]Mindich Child Health and Development Institute and Departments of Pediatrics and Genetics and Genomic Sciences, Icahn School of Medicine at Mount Sinai, New York, NY.

[¶]These authors jointly directed this work.

[*]Correspondence to:

Simone Martinelli, Dipartimento di Ematologia, Oncologia e Medicina Molecolare, Istituto Superiore di Sanità, Viale Regina Elena, 299, Rome 00161, Italy. E-mail: simone.martinelli@iss.it

Marco Tartaglia, Genetics and Rare Diseases Research Division, Ospedale Pediatrico Bambino Gesù, IRCCS, Viale di San Paolo, 15, Rome 00146, Italy. E-mail: marco.tartaglia@opbg.net

Contract grant sponsors:

Telethon-Italy (GGP13107), Associazione Italiana per la Ricerca sul Cancro (IG 17583), Italian Ministry of Health (RF-2011-02349938 and RC-2016) to MT; ERA-Net for Research Programmes on Rare Diseases (NSEuroNet) to HC, MZ and MT; Ministero dell'Istruzione, dell'Università e della Ricerca (PRIN 2010NRREPL_008 and PRIN 2015_7WW5EH) to LS. MA was supported by Fondazione Umberto Veronesi and Associazione Italiana Sindrome di Costello e cardiofaciocutanea.

Abstract

Germline mutations in *PTPN11*, the gene encoding the Src-homology 2 (SH2) domain-containing protein tyrosine phosphatase (SHP2), cause Noonan syndrome (NS), a relatively common, clinically variable, multisystem disorder. Here, we report on the identification of five different *PTPN11* missense changes affecting residues Leu^{261}, Leu^{262} and Arg^{265} in 16 unrelated individuals with clinical diagnosis of NS or with features suggestive for this disorder, specifying a novel disease-causing mutation cluster. Expression of the mutant proteins in HEK293T cells documented their activating role on MAPK signaling. Structural data predicted a gain-of-function role of substitutions at residues Leu^{262} and Arg^{265} exerted by disruption of the N-SH2/PTP autoinhibitory interaction. Molecular dynamics simulations suggested a more complex behavior for changes affecting Leu^{261}, with possible impact on SHP2's catalytic activity/selectivity and proper interaction of the PTP domain with the regulatory SH2 domains. Consistent with that, biochemical data indicated that substitutions at codons 262 and 265 increased the catalytic activity of the phosphatase, while those affecting codon 261 were only moderately activating but impacted substrate specificity. Remarkably, these mutations underlie a relatively mild form of NS characterized by low prevalence of cardiac defects, short stature, and cognitive and behavioral issues, as well as less evident typical facial features.

Key Words: *PTPN11* mutations; Noonan syndrome; structural and functional studies; genotype-phenotype correlation analysis

Introduction

PTPN11 (MIM# 176876) encodes the non-receptor Src homology 2 (SH2) domain-containing protein tyrosine phosphatase 2 (SHP2), a widely expressed signal transducer implicated in multiple intracellular signaling pathways, including the RAS-MAPK and PI3K-AKT cascades [Tartaglia et al., 2004a; Tajan et al., 2015]. Heterozygous germline mutations in *PTPN11* cause Noonan syndrome (NS, MIM# 163950) [Tartaglia et al., 2001, 2002] and the clinically related NS with multiple lentigines (NSML, MIM# 151100; previously known as LEOPARD syndrome) [Digilio et al., 2002; Legius et al., 2002], two developmental disorders characterized by reduced postnatal growth, congenital heart disease, hypertrophic cardiomyopathy (HCM), facial dysmorphisms, variable cognitive deficits, and skeletal, hematological and lymphatic anomalies [Tartaglia et al., 2011; Roberts et al., 2013]. A third class of mutations occurs as somatic events with variable prevalence in childhood myeloproliferative and myelodysplastic disorders, as well as leukemias [Tartaglia et al., 2003, 2004b, 2006]. Furthermore, loss-of-function (LoF) mutations in the same gene have more recently been associated with the dominantly transmitted metachondromatosis (MIM# 156250), a rare cartilage tumor-predisposing syndrome characterized by multiple exostoses, enchondromas and skeletal abnormalities, wherein a second somatic hit results in complete SHP2's LoF in affected cells [Bowen et al., 2011].

SHP2 contains two tandemly arranged *N*-terminal SH2 domains (N-SH2 and C-SH2), followed by a catalytic PTP domain and a *C*-terminal tail with a still largely uncharacterized function (Fig. 1A). SHP2's activity and subcellular localization is controlled by an allosteric switch involving the N-SH2 and PTP domains [Hof et al., 1998]. Under basal conditions, the catalytically inactive conformation of the phosphatase is stabilized by a wide intramolecular binding network involving residues located at the N-SH2/PTP interface. Binding of phosphotyrosine (pY)-containing signaling partners at a different site of the N-SH2 domain

promotes the release of this autoinhibitory interaction, making the catalytic site available to substrates. The spectrum of disease-causing *PTPN11* mutations has been thoroughly characterized [Tartaglia et al., 2006; Strullu et al., 2014]. Most mutations underlying NS or contributing to hematologic malignancies cluster at the N-SH2/PTP interface. These activating lesions are known to destabilize the autoinhibitory interactions between these two domains, enhancing basal phosphatase activity and affinity for binding partners [Keilhack et al., 2005; Tartaglia et al., 2006]. Other lesions localize within the region of the SH2 domains mediating SHP2's interaction to signaling partners, increasing binding affinity or changing binding selectivity [Martinelli et al., 2008]. Biochemical and functional characterization of these changes confirmed their activating role on SHP2's function and the MAPK cascade [Kontaridis et al., 2006; Martinelli et al., 2012]. In contrast, NSML-associated mutations dramatically affect the catalytic activity of the enzyme [Keilhack et al., 2005; Hanna et al., 2006; Kontaridis et al., 2006; Tartaglia et al., 2006; Martinelli et al., 2008], and promote enhanced PI3K-AKT signaling [Edouard et al., 2010]. The effects of mutations on the functional regulation of SHP2, however, can be more complex [Martinelli et al., 2012], and the precise structural and functional consequences of many of these lesions remain to be elucidated.

Here, we report on a novel *PTPN11* mutation cluster causing NS, and provide data on the effects of those lesions on SHP2's structure and function, and their associated clinical phenotype.

Materials and Methods

Patients. Mutation scanning of *PTPN11* was performed in a diagnostic setting on cohorts of subjects with a clinical diagnosis of NS or NSML by partners of the NSEuroNet Consortium (MT, HC and MZ) and their associated external collaborators. Clinical assessment was performed by experienced pediatricians and clinical geneticists. DNA samples and clinical data were collected following institutional review board-approved protocols, and written informed consent for genetic analyses was obtained from all patients or their legal guardians.

Molecular Data. Genomic DNA was isolated from circulating leukocytes by using standard techniques. The entire *PTPN11* coding sequence, together with the exon/intron boundaries and their flanking intronic regions were scanned for mutations by either Sanger sequencing or parallel targeted resequencing. Sanger sequencing used ABI BigDye Terminator Sequencing chemistry (Applied Biosystems) and ABI 3700/3500 Capillary Array Sequencers (Applied Biosystems). Massive parallel resequencing was performed on MiSeq (Illumina) and PGM (Life Technologies) platforms, using different custom panels designed to target coding exons and flanking intronic sequences of most of the known NS/NSML genes, as well as genes causing clinically related phenotypes (*i.e.*, *PTPN11*, *CBL*, *SOS1*, *SHOC2*, *NF1*, *SPRED1*, *KRAS*, *HRAS*, *NRAS*, *RAF1*, *BRAF*, *MAP2K1*, *MAP2K2*, and *RIT1*). Average coverage of target regions was >98.5%, with average sequencing depth on target of 452x. Details on panels and sequencing protocols are available upon request.

The identified mutations have been submitted to the NS EuroNet database (https://nseuronet.com/php/index.php). To determine the in *cis*/*trans status* of the c.781C>T and c.794G>A missense changes identified to co-occur as *de novo* events in subject ADL1, exon 7 was PCR-amplified and subcloned (pCR2.11-TOPO1TA vector, Life Technologies).

The insert of 12 independent clones was sequenced to resolve the haplotype in individual clones.

Exact confidence intervals of proportions (at 95% level) were calculated based on the binomial distribution.

Structural Analyses and Molecular Dynamics (MD) Simulations. Structural analyses were based on the structure of SHP2 in its autoinhibited conformation (PDB code 2SHP), after modeling the missing regions, as previously described [Bocchinfuso et al., 2007]. Residues located at the surface of the PTP domain interacting with the N-SH2 and C-SH2 domains and the linker connecting these domains were defined by calculating change in solvent accessible surface (SAS) following removing the SH2 domains. SAS values are reported as a percent of the total surface of residues of interest. Calculations were performed with MOLMOL [Koradi et al., 1996]. Interdomain interactions were also considered in a model of the active state of SHP2, obtained by homology modeling using the structure of SHP1 (PDB code 3PS5) by SwissModel server [Arnold et al., 2006; https://swissmodel.expasy.org].

For MD simulations, mutations were introduced by means of the Swiss-PdbViewer software version 4.1 [Guex and Peitsch, 1997; http://spdbv.vital-it.ch] and the rotamers were chosen based on the favorable contacts with the rest of the protein and the corresponding potential energies. SHP2 was positioned at the center of a dodecahedral box and solvated with ~23000 explicit water molecules. Three Na^+ counterions were added to provide a neutral simulation box. The solvent was relaxed by two energy minimization steps and a 300 ps MD simulation at 300 K (velocities were randomly assigned according to a Maxwellian distribution), while restraining the protein atomic positions with a harmonic potential of 10 kJ/(mol $Å^2$). After removing restraints, another minimization was performed, and the temperature of the system was brought from 50 K to 300 K in a step-wise manner (totally 4 ns of simulations). A productive run of 100 ns was carried out for wild-type SHP2 and the

p.L261F and p.L261H mutants. The last 50 ns were then used for subsequent analysis. MD calculations were carried out with Gromacs software package version 4.6 [Hess et al., 2008a] by using AMBER99sb force field [Hornak et al., 2006]. The P-LINCS method [Hess, 2008b] was applied to constrain covalent bond lengths, allowing an integration step of 2 fs. Electrostatic interactions were calculated with the Particle-Mesh Ewald method [Darden and Pedersen, 1993]. The temperature was controlled by separately coupling the protein and solvent to an external temperature bath [Bussi et al., 2007], by using weak coupling for pressure [Berendsen et al., 1984]. For each atom, B-factors were calculated by using the g_rmsf routine in the GROMACS software package. A salt bridge was assigned whenever the minimum distance between the charged groups of the involved residue fell below 0.4 nm. Molecular graphics were created with the UCSF Chimera software version 1.10 [Pettersen et al., 2004; https://www.cgl.ucsf.edu/chimera].

Expression Constructs. The human full-length polyHis-tagged *PTPN11* cDNA was cloned in a pET-26b vector (Novagen) using the *Hind*III and *Xho*I restriction sites. Relevant nucleotide substitutions at codons Leu^{261}, Leu^{262}, Arg^{265} and Ala^{72} were introduced by site-directed mutagenesis (QuikChange site-directed mutagenesis kit, Stratagene). Constructs containing the isolated PTP domain (residues 212-541) were generated by PCR amplification of the full-length wild-type construct (forward primer: 5'-CACACAAAGCTTCTCAAGCAGCCCCTTAACACG-3'; reverse primer: 5'-CACACACTCGAGTTCGTGCCCTTTCCTCTTGC-3'), and subcloned into the pET-26b vector. For cell transfection studies, full-length *PTPN11* cDNAs were cloned in pcDNA6/V5-HisA (Invitrogen). The coding sequence of all constructs was confirmed by Sanger sequencing.

ERK and AKT Phosphorylation Assay. HEK293T cells were cultured in Dulbecco's modified Eagle's medium (VWR International PBI) supplemented with 10% heat-inactivated fetal bovine serum (EuroClone) and 1% penicillin-streptomycin, at 37 °C with 5% CO_2. Cells were seeded in six-well plates the day before transfection. Monolayers were transfected at 70% confluency by using *Fugene 6* transfection reagent (Promega), with constructs encoding the V5-tagged wild-type or mutant SHP2 proteins, together with a FLAG-Gab1 plasmid [Fragale et al., 2004]. Twenty-four hours after transfection, cells were serum-starved for 24 h, and treated with 30, 60 or 100 ng/ml EGF (Invitrogen) for 5 or 15 min, or left unstimulated. ERK and AKT activation was assessed on total cell lysates by using anti-phospho-44/42 ERK (Thr202/Tyr204) and anti-phospho AKT antibodies (Cell Signaling). Membranes were then stripped and re-probed with anti-GAPDH (Santa Cruz), anti-44/42 ERK (Cell Signaling) and anti-AKT (Cell Signaling) antibodies for protein normalization. To evaluate SHP2-V5 and FLAG-Gab1 protein levels, 10 µg of total lysates were immunoblotted with anti-V5 (Invitrogen) and anti-FLAG (Sigma) antibodies. After washing, membranes were incubated with the secondary antibodies (Pierce), and immunoreactive bands were visualized using SuperSignal Chemiluminescent Substrate (Thermo Scientific).

Protein Purification. Recombinant proteins were expressed as reported previously [Martinelli et al., 2008], using *E. coli* (DE3) Rosetta2-competent cells (Novagen). Briefly, following IPTG induction (2 h at 30 °C), harvesting, and cell lysis, polyHis-tagged full-length SHP2 proteins and isolated PTP domains ($SHP2_{PTP}$) were purified by chromatography, using nickel-nitrilotriacetic acid magnetic agarose beads (Qiagen), and stored at -20 °C in the presence of 5 mM DTT (Sigma).

Phosphatase Assays. Catalytic activity of wild-type SHP2 and NS-causing mutants was evaluated *in vitro* using 20 pmol of recombinant proteins and 20 mM *p*-nitrophenyl

phosphate (pNPP) (Sigma) as substrate, either in basal condition or in presence of the protein-tyrosine phosphatase nonreceptor type substrate 1 (PTPNS1) bisphosphotyrosyl-containing activation motif (BTAM peptide) (GGGGDIT(pY)ADLNLPKGKKPAPQAAEPNNHTE(pY)ASIQTS) (Primm), as previously described [Martinelli et al., 2012]. Proteins were incubated at 30 °C (30 min for full-length SHP2; 15 min for $SHP2_{PTP}$). Phosphate release was determined by measuring A_{405}. Amount, purity, and integrity of recombinant proteins were assessed by protein assay kit (BioRad) and Coomassie Blue staining.

Substrate specificity was evaluated through a malachite green phosphate assay kit (Millipore) using the DKQVEpYLDLDL, EEENIpYSVPHD and VDADEpYLIPQQ phosphopeptides (Primm), which derived from known SHP2 substrates ($GAB1_{Y657}$, $p190A/RhoGAP_{Y1105}$, and $EGFR_{Y1016}$, respectively) [Sun et al., 2009; Ren et al., 2011]. Wild-type and mutant $SHP2_{PTP}$ (3.6 nM) were incubated with 300 µM of each phosphopeptide for 1 min. The reaction was stopped by adding 100 µl of malachite green solution. After 15 min, absorbance was read at 655 nm by using a microplate reader, and compared to a phosphate standard curve to determine the release of phosphate.

Results

Identification of a novel *PTPN11* mutation cluster causing NS

Among approximately 1500 subjects with clinical diagnosis of NS or NSML screened in centers participating in the NSEuroNet Consortium, found to carry heterozygous mutations in *PTPN11*, five different missense changes affecting residues Leu^{261}, Leu^{262} and Arg^{265} were identified in 16 unrelated individuals (NS EuroNet database, https://nseuronet.com/php/index.php). These variants accounted approximately for 1% (95% CI, 0.6%-1.6%) of cases, specifying a novel mutation cluster causing NS (Table 1). All mutations were novel, the only exception being the c.781C>T transition (p.L261F) that had previously been reported in one NS patient [Ezquieta et al., 2012]. This lesion, as well as the c.785T>G (p.L262R) and c.794G>A (p.R265Q) changes were shown to occur as *de novo* events by genotyping of parental DNAs in seven cases, while they co-segregated with the disease in four families. Similarly, the c.782T>A (p.L261H) and c.784C>T (p.L262F) substitutions co-segregated with the trait in single families. The c.781C>T and c.794G>A transitions were also found to co-occur as *de novo* events in one patient. In this case, exon 7 was PCR-amplified, cloned, and the insert of 12 independent clones was sequenced, identifying seven clones representing the reference allele and five clones carrying both variants, indicating that these lesions occurred in *cis*.

All variants were considered to be pathogenic for the following reasons. First, they arose as *de novo* events in several patients. Second, they were not reported in public databases or occurred with a frequency below 1/20000 in the Exome Aggregation Consortium's database (ExAC; http://exac.broadinstitute.org). Third, they were non-conservative, affected highly conserved residues among *PTPN11* orthologs in vertebrates (Supp. Fig. S1), and were predicted to be "deleterious" by Combined Annotation Dependent Depletion (CADD) v.1.3 [Kircher et al., 2014], Database for Nonsynonymous SNPs'

Functional Predictions (dbNSFP) Support Vector Machine (SVM) v.3.0 [Dong et al., 2015] and REVEL [Ioannidis et al., 2016] algorithms (Table 1). Finally, the three affected residues are located in close spatial proximity to residues previously identified to be mutated in NS (*i.e.*, Gln^{256} and Gly^{268}). Based on these considerations and their biochemical/functional impact *in vitro* (see below), all changes but c.782T>A (p.L261H) satisfied the criteria to be considered pathogenic according to the ACMG guidelines [Richards et al., 2015].

Structural analyses

Based on their clinical relevance, *in silico* analyses were performed to explore the consequences of the identified mutations on protein structure and function. Residues Leu^{261}, Leu^{262} and Arg^{265} are located within the PTP domain, in a region comprising helices B (residues 247-261) and C (residues 265-269) [Hof et al., 1998] (Fig. 1A and B). In a homology model for an open state of the phosphatase based on the X-ray structure of SHP1 in a putative active state [Wang et al., 2011], this region does not participate in any interdomain interaction (data not shown). In SHP2's inactive structure, however, this region, particularly helix B, is involved in a complex interdomain binding network. Specifically, it interacts directly with the catalytic site, the N-SH2 domain, as well as with the linker connecting the N-SH2 and C-SH2 domains, which stabilizes the relative orientation of the C-SH2 domain. Importantly, in the autoinhibited conformation of the phosphatase, the side chains of Leu^{262} and Arg^{265} participate directly to the N-SH2/PTP interface binding network (Fig. 1C and D). Coherently, after removal of the SH2 domains, the SAS value for Leu^{262} and Arg^{265} increases from 15% to 53% and from 9% to 18%, respectively. In particular, these residues are in tight contact with Glu^{76}, whose mutations cause NS and hematologic malignancies by destabilizing the closed, inactive conformation of the enzyme [Tartaglia et al., 2006; Bocchinfuso et al., 2007]. Leu^{262} also interacts with Ala^{75} and Gln^{79}, the latter being mutated in roughly 4% of *PTPN11* mutation-positive NS cases [Tartaglia et al., 2006]. Based

on these considerations, substitutions affecting residues 262 and 265 are predicted to destabilize the closed conformation of the protein, leading to increased basal activity and responsiveness to binding partners. Different from those findings, the SAS value for Leu^{261} is only 5% of its total surface, and is not affected by removal of the SH2 domains (6%). The side chain of Leu^{261} points towards the PTP core, and forms a hydrophobic cluster with the aliphatic portions of residues of the B-helix (Gln^{257}, Glu^{258}, and Lys^{260}), Tyr^{263} and Phe^{285}, and two residues belonging to the H-helix (Gln^{495} and Arg^{498}) (Fig. 1E). This extended network of interactions suggests a role for Leu^{261} in the stabilization of the B-helix orientation. Considering the centrality of this helix in both the structural organization of the PTP active site and stabilization of the inactive conformation of the phosphatase, mutations at residue Leu^{261} were predicted to perturb SHP2's function by a more complex mechanism.

To characterize such perturbing effect(s), MD simulations were carried out on the entire wild-type SHP2 and mutants at codon 261. Although substitutions at this residue did not cause large-scale conformational changes, a different flexibility of the PTP domain active site was observed in the mutant proteins (Fig. 2), particularly in regions participating in substrate recognition and catalysis, including the B-helix, predicting an effect of these lesions on the catalytic activity and/or selectivity of the PTP domain. A slightly different behavior at the PTP/N-SH2 interface was also observed. Specifically, the salt-bridge involving residues Lys^{35} and Asp^{241} appeared to be weaker or absent in the simulations trajectories of $SHP2^{L261H}$ and $SHP2^{L261F}$, respectively. Overall, these data suggest that amino acid substitutions at codon 261 might perturb both the dynamic features of the PTP domain and the N-SH2/PTP interaction.

Activity of SHP2 mutants

SHP2 positively modulates MAPK signaling, and NS-causing and leukemia-associated *PTPN11* mutations have been documented to enhance intracellular signaling through this

cascade. To test whether the identified mutations were activating, their impact on ERK phosphorylation was assessed. Ectopic expression of the V5-tagged SHP2^{L261F}, SHP2^{L262F}, SHP2^{L262R}, and SHP2^{R265Q} mutants in HEK293 cells was found to promote variably enhanced ERK phosphorylation upon 30 ng/ml EGF stimulation, compared to what observed in cells overexpressing the wild-type enzyme, providing evidence for their activating role on the MAPK signaling cascade (Fig. 3). In contrast, the SHP2^{L261H} mutant was documented to enhance ERK phosphorylation when cells were treated with higher doses of growth factor and behaved as the most activating mutant following stimulation with 100 ng/ml EGF (Supp. Fig. S2), suggesting either a quantitatively milder or qualitatively distinct activating effect on MAPK signaling.

To explore the consequences of these lesions on protein function, the corresponding mutants were expressed in bacteria, purified and their phosphatase activity was determined *in vitro*, basally and following stimulation with a BTAM peptide previously shown to activate SHP2 [Tartaglia et al., 2006; Martinelli et al., 2012]. For comparison, the wild-type enzyme and the leukemia-associated SHP2^{A72V} mutant were also tested. Under basal conditions, SHP2^{L262R}, SHP2^{R265Q} and the SHP2$^{L261F/R265Q}$ double mutant exhibited a slightly increased substrate dephosphorylation compared to the wild-type protein (Student's *t*-test, $P < 0.01$) (Fig. 4A). As expected, their phosphatase activity was significantly lower compared with that observed for the oncogenic mutant. Following BTAM peptide stimulation, however, all mutants at those codons displayed enhanced catalytic activation ($P < 0.001$, in all comparisons), indicating that these changes stabilize SHP2 in its open, active state.

Among mutants at codon 261, SHP2^{L261H} showed a slightly increased basal activity ($P < 0.01$), suggesting a weak perturbing effect of this lesion on the autoinhibited conformation of SHP2 (Fig. 4A). Following BTAM stimulation, both mutants displayed enhanced activation ($P < 0.01$) that was, however, considerably lower compared with that generally

observed in proteins carrying mutations at the N-SH2/PTP interface, including those at codons 262 and 265 (Fig. 4A). To further characterize the biochemical behavior of the $SHP2^{L261F}$ and $SHP2^{L261H}$ proteins, their catalytic activity was measured as a function of BTAM peptide concentration, which documented enhanced responsiveness of both mutants at high doses of phosphopeptide, compared to the wild-type enzyme (Fig. 4B). To test whether such a hyperactive behavior might be related to enhanced catalytic capability, the intrinsic phosphatase activities were assayed by introducing each mutation into a construct encoding for the isolated PTP domain ($SHP2_{PTP}$). Phosphatase assays demonstrated no significant changes in catalysis compared to wild-type SHP2 (Fig. 4C). Finally, to explore the possibility that lesions at codon 261 might affect substrate specificity, the activity of wild-type and mutated PTP domains was assessed against three selected phosphopeptides containing the tyrosine phosphorylation sites of GAB1 (Tyr^{657}), p190A/RhoGAP (Tyr^{1105}), and EGFR (Tyr^{1016}), known to represent targets of the phosphatase [Sun et al., 2009; Ren et al., 2011]. Consistent with our structural findings, slightly, but significantly, altered activity was observed using GAB1 as substrate (P <0.05, in both comparisons), indicating a possible impact of mutations at codon 261 on substrate selectivity (Fig. 4D). Based on this finding and the observation that a different class of *PTPN11* mutations implicated in NSML has been shown to upregulate PI3K/AKT signaling [Edouard et al., 2010], a possible differential impact of these mutations on AKT phosphorylation was evaluated. Both mutants at codon 261, however, did not impact on the PI3K-AKT signaling pathway (data not shown), which is consistent with the clinical features observed in the eight subjects heterozygous for a missense change affecting Leu^{261}.

Phenotypic spectrum associated with mutations at codons 261, 262 and 265

Extensive clinical data were available for all probands and four affected relatives (Supp. Table S1). Photographs were available for two sporadic cases, and a child and his affected

mother (Supp. Fig. S3). Genotype-phenotype correlation analyses revealed that lesions affecting residues 261, 262 and 265 are associated with a relatively variable phenotype within the NS phenotypic spectrum. Notably, clinical features were quite subtle in the majority of cases (Supp. Table S1 and S2). In particular, we noticed a significant lower prevalence of cardiac defects compared to what observed among *PTPN11* mutation-positive patients (9/19 *vs*. 236/285, P <0.001; two-tail Fisher's exact test) and the general NS population (132/151, P <0.001) [Sarkozy et al., 2009]. Restricting our analysis to NS cases with *PTPN11* mutations, we recorded a lower prevalence of pulmonary valve stenosis, which occurred only in 37% of cases (7/19 *vs*. 247/362, P <0.02). None of these patients exhibited HCM. A relatively low prevalence of short stature and less evident typical facial features (*i.e.*, low recurrence of palpebral ptosis and dysmorphic/low set ears) were also documented. Finally, no significant cognitive and behavioral issues were observed in the subset of subjects carrying a mutation at residue Leu^{261}.

Discussion

Noonan syndrome is among the most common non-chromosomal disease affecting development and growth. In approximately half of affected subjects, the disorder is caused by mutations in *PTPN11*. Multiple classes of *PTPN11* mutations with a distinct perturbing effect on SHP2's function have been identified. Consistent with such variable impact, *PTPN11* mutations have been established to underlie or contribute to different human diseases, including childhood hematologic malignancies. Here, we report on the identification, and structural and functional characterization of a novel cluster of germline missense mutations in *PTPN11* underlying NS. The new mutation cluster affects a region of the PTP domain of SHP2 involved in extensive inter- and intra-domain interactions. The collected data documented an heterogeneous impact of mutations involving these adjacent residues on protein function and intracellular signaling, which was, however, associated with an overall relatively mild phenotype characterized by low prevalence of cardiac defects, reduced growth, and cognitive and behavioral issues, as well as less evident typical facial features.

According to the crystallographic structure of SHP2 and the proposed mechanism of activation [Hof et al., 1998], *PTPN11* mutations have been classified into six major groups [Tartaglia et al., 2006]. Groups I and II comprise lesions affecting the N-SH2/PTP interface, participating (group II) or not (group I) in catalysis. Changes belonging to group III and IV affect residues mediating substrate specificity or with a role in maintaining the overall PTP structure, respectively. Group V mutations involve residues located at the binding cleft of each SH2 domain. Finally, group VI includes lesions affecting amino acids located within the linker stretch connecting the N-SH2 and C-SH2 domains. The novel mutation cluster here described affects residues located in the B-helix (Leu^{261}) and the following unstructured segment (Leu^{262} and Arg^{265}) of the PTP domain, a region whose role has not been characterized yet. Although the novel mutations are in tight contiguity along the PTP domain,

structural analysis and biochemical data unexpectedly demonstrated that they act through different molecular mechanisms. Similar to the majority of *PTPN11* mutations causing NS and leukemia, substitutions at residues Leu^{262} and Arg^{265} affect the N-SH2/PTP interacting surface and enhance SHP2's function by perturbing the autoinhibitory interaction between these two domains. Consistent with that, the collected biochemical data support the idea that mutations at codons 262 and 265 behave as typical group I lesions. The biochemical behavior of *PTPN11* mutations, however, can be more complex. For instance, the molecular mechanism underlying the pathogenicity of the p.Tyr62Asp and p.Tyr63Cys amino acid changes implies balancing of two counteracting effects operating on the allosteric control of SHP2's function, one affecting the stability of the inactive conformation of the protein, the other perturbing the structure and function of the pY-binding cleft mediating SHP2's binding to signaling partners [Martinelli et al., 2012]. Likewise, the upregulated SHP2's function linked to the p.I282V substitution is the result of a mild disruption of the N-SH2/PTP interaction combined to enhanced intrinsic catalytic activity [Martinelli et al., 2008]. As observed for those mutations, the collected structural and biochemical data suggest that the missense changes affecting Leu^{261} belong to group IV and likely exert their pathogenic effect by perturbing SHP2's function at different levels. Leu^{261} is part of a hydrophobic core including Phe^{285} and Arg^{498}, which are in tight contact with residues surrounding the active site of the protein that play a key role in controlling substrate specificity [Andersen et al., 2001], and whose mutations cause NS and NSML, respectively [Tartaglia et al., 2006]. MD simulations performed on the whole protein allowed us to appreciate that the NS-associated substitutions at this codon altered the hydrophobic cluster which, in turn, was predicted to affect the mobility of key regions of the PTP domain, including those directly involved in PTP selectivity. Of note, such diverse flexibility of the PTP active site was also shown to possibly impact on the interaction with the N-SH2 domain. Overall, the collected data

suggest that these mutations are likely to perturb SHP2's function by altering the interdomain interactions and the intramolecular binding network mediating substrate recognition. Of note, Leu^{261} is not conserved among human PTP domains [Andersen et al., 2001], suggesting that amino acid substitutions at this position have a perturbing role specifically on SHP2, rather than exerting a general disruptive effect on the catalytic function.

Based on their consequences on SHP2's structure and function, their variable activating effect on the MAPK signaling cascade, and their *de novo* origin in several instances, most changes affecting the novel mutation cluster can be considered as *bona fide* mutations causing NS. Among these, however, the missense change predicting the p.L261H substitution was identified only in one familial case. For this variant, the evidence provided by the *in silico* data was not unambiguously supported by the experimental data, which were indicative of enhanced activity of the mutant only at high phosphopeptide concentrations *in vitro*, and demonstrated a significant upregulation of signaling through the MAPK cascade in transiently transfected cells only when they were treated with high doses of EGF. Based on these considerations, we deem the c.781C>T substitution as a functionally relevant change with mild clinical impact, even though, in the absence of any additional evidence supporting pathogenicity, this change should formally be classified as a variant of unknown significance.

The clinical features associated with *PTPN11* mutations at codons 261, 262 and 265 undoubtedly fall within the NS phenotypic spectrum. Genotype-phenotype correlation analysis revealed that affected subjects exhibit a relatively lower prevalence of cardiac defects (47%) compared with both *PTPN11*-positive (83%) and *PTPN11*-negative (64%) NS populations [Sarkozy et al., 2009]. Among individuals with a mutation affecting those residues, a significantly lower prevalence of pulmonary valve stenosis compared to what generally observed among NS patients with *PTPN11* mutations was observed (37% vs 68%, $P < 0.02$). A major finding also regarded the relatively lower prevalence of short

stature/length below the third centile in these subjects (60%) compared with *PTPN11* mutation-positive NS cases (76-93%) [Sarkozy et al., 2009; Roberts et al., 2013]. Finally, a mild phenotype was particularly noted in subjects heterozygous for mutations affecting Leu^{261}. While this genotype-phenotype correlation seems to be consistent with the apparently moderate functional impact of mutations involving that residue, a higher number of cases is required to confirm this observation.

Overall, this report provides clinical and functional data on a previously unrecognized mutation cluster affecting residues Leu^{261}, Leu^{262} and Arg^{265}. Recently, Chen and colleagues identified a novel class of inhibitors able to stabilize SHP2 in its inactive state by binding the phosphatase in close proximity to the B-helix. Besides the promising clinical relevance of this study, these findings suggest a fine tuning role of this region in the allosteric regulation of the enzyme [Chen et al., 2016], a picture that is further supported by the present findings.

Acknowledgments

We are grateful to the individuals and their families who contributed to this study. We thank Serenella Venanzi (ISS, Rome, Italy) for skillful technical assistance. We also thank the CINECA consortium for providing computational resources.

References

Andersen JN, Mortensen OH, Peters GH, Drake PG, Iversen LF, Olsen OH, Jansen PG, Andersen HS, Tonks NK, Møller NP. 2001. Structural and evolutionary relationships among protein tyrosine phosphatase domains. Mol Cell Biol 21(21): 7117-36.

Arnold K, Bordoli L, Kopp J, Schwede T. 2006. The SWISS-MODEL workspace: a web-based environment for protein structure homology modelling. Bioinformatics 22(2): 195-201.

Berendsen HJC, Postma JPM, van Gunsteren WF, DiNola A, Haak JR. 1984. Molecular dynamics with coupling to an external bath. J Chem Phys 81: 3684

Bocchinfuso G, Stella L, Martinelli S, Flex E, Carta C, Pantaleoni F, Pispisa B, Venanzi M, Tartaglia M, Palleschi A. 2007. Structural and functional effects of disease-causing amino acid substitutions affecting residues Ala72 and Glu76 of the protein tyrosine phosphatase SHP-2. Proteins 66(4): 963-74.

Bowen ME, Boyden ED, Holm IA, Campos-Xavier B, Bonafé L, Superti-Furga A, Ikegawa S, Cormier-Daire V, Bovée JV, Pansuriya TC, de Sousa SB, Savarirayan R, et al. 2011. Loss-of-function mutations in PTPN11 cause metachondromatosis, but not Ollier disease or Maffucci syndrome. PLoS Genet 7(4): e1002050. doi: 10.1371/journal.pgen.1002050.

Bussi G, Donadio D, Parrinello M. 2007. Canonical sampling through velocity rescaling. J Chem Phys 126(1): 014101.

Chen YN, LaMarche MJ, Chan HM, Fekkes P, Garcia-Fortanet J, Acker MG, Antonakos B, Chen CH, Chen Z, Cooke VG, Dobson JR, Deng Z, et al. 2016. Allosteric inhibition of SHP2 phosphatase inhibits cancers driven by receptor tyrosine kinases. Nature 535(7610): 148-52.

Darden TA, Pedersen LG. 1993. Molecular modeling: an experimental tool. Environ Health Perspect 101(5): 410-2.

Digilio MC, Conti E, Sarkozy A, Mingarelli R, Dottorini T, Marino B, Pizzuti A, Dallapiccola B. 2002. Grouping of multiple-lentigines/LEOPARD and Noonan syndromes on the PTPN11 gene. Am J Hum Genet 71(2): 389-94.

Dong C, Wei P, Jian X, Gibbs R, Boerwinkle E,Wang K, Liu X. 2015. Comparison and integration of deleteriousness prediction methods for nonsynonymous SNVs in whole exome sequencing studies. Hum Mol Genet 24(8):2125-37.

Edouard T, Combier JP, Nédélec A, Bel-Vialar S, Métrich M, Conte-Auriol F, Lyonnet S, Parfait B, Tauber M, Salles JP, Lezoualc'h F, Yart A, et al. 2010. Functional effects of PTPN11 (SHP2) mutations causing LEOPARD syndrome on epidermal growth factor-induced phosphoinositide 3-kinase/AKT/glycogen synthase kinase 3beta signaling. Mol Cell Biol 30(10): 2498-507.

Ezquieta B, Santomé JL, Carcavilla A, Guillén-Navarro E, Pérez-Aytés A, Sánchez del Pozo J, García-Miñaur S, Castillo E, Alonso M, Vendrell T, Santana A, Maroto E, et al. 2012. Alterations in RAS-MAPK genes in 200 Spanish patients with Noonan and other neuro-cardio-facio-cutaneous syndromes. Genotype and cardiopathy. Rev Esp Cardiol (Engl Ed). 65(5): 447-55.

Fragale A, Tartaglia M, Wu J, Gelb BD. 2004. Noonan syndrome-associated SHP2/PTPN11 mutants cause EGF-dependent prolonged GAB1 binding and sustained ERK2/MAPK1 activation. Hum Mutat 23(3): 267-77.

Guex N, Peitsch MC. 1997. SWISS-MODEL and the Swiss-PdbViewer: an environment for comparative protein modeling. Electrophoresis 18(15): 2714-23.

Hanna N, Montagner A, Lee WH, Miteva M, Vidal M, Vidaud M, Parfait B, Raynal P. 2006. Reduced phosphatase activity of SHP-2 in LEOPARD syndrome: consequences for PI3K binding on Gab1. FEBS Lett 580(10): 2477-82.

Hess B, Kutzner C, van der Spoel D, Lindahl E. 2008a. GROMACS 4: Algorithms for Highly Efficient, Load-Balanced, and Scalable Molecular Simulation. J Chem Theory Comput 4(3): 435-47.

Hess B. 2008b. P-LINCS: A Parallel Linear Constraint Solver for Molecular Simulation. J Chem Theory Comput 4(1): 116-22.

Hof P, Pluskey S, Dhe-Paganon S, Eck MJ, Shoelson SE. 1998. Crystal structure of the tyrosine phosphatase SHP-2. Cell 92(4): 441-50.

Hornak V, Abel R, Okur A, Strockbine B, Roitberg A, Simmerling C. 2006. Comparison of multiple AMBER force fields and development of improved protein backbone parameters. Proteins 65(3):712-25.

Ioannidis NM, Rothstein JH, Pejaver V, Middha S, McDonnell SK, Baheti S, Musolf A, Li Q, Holzinger E, Karyadi D, Cannon-Albright LA, Teerlink CC, et al. 2016. REVEL: An Ensemble Method for Predicting the Pathogenicity of Rare Missense Variants. Am J Hum Genet 99(4):877-85.

Keilhack H, David FS, McGregor M, Cantley LC, Neel BG. 2005. Diverse biochemical properties of Shp2 mutants. Implications for disease phenotypes. J Biol Chem 280(35): 30984-93.

Kircher M, Witten DM, Jain P, O'Roak BJ, Cooper GM, Shendure J. 2014. A general framework for estimating the relative pathogenicity of human genetic variants. Nat Genet 46(3):310-5.

Kontaridis MI, Swanson KD, David FS, Barford D, Neel BG. 2006. PTPN11 (Shp2) mutations in LEOPARD syndrome have dominant negative, not activating, effects. J Biol Chem 281(10): 6785-92.

Koradi R, Billeter M, Wüthrich K. 1996. MOLMOL: a program for display and analysis of macromolecular structures. J Mol Graph 14(1): 51-5, 29-32.

Legius E, Schrander-Stumpel C, Schollen E, Pulles-Heintzberger C, Gewillig M, Fryns JP. 2002. PTPN11 mutations in LEOPARD syndrome. J Med Genet 39(8): 571-4.

Martinelli S, Torreri P, Tinti M, Stella L, Bocchinfuso G, Flex E, Grottesi A, Ceccarini M, Palleschi A, Cesareni G, Castagnoli L, Petrucci TC, et al. 2008. Diverse driving forces underlie the invariant occurrence of the T42A, E139D, I282V and T468M SHP2 amino acid substitutions causing Noonan and LEOPARD syndromes. Hum Mol Genet 17(13): 2018-29.

Martinelli S, Nardozza AP, Delle Vigne S, Sabetta G, Torreri P, Bocchinfuso G, Flex E, Venanzi S, Palleschi A, Gelb BD, Cesareni G, Stella L, et al. 2012. Counteracting effects operating on Src homology 2 domain-containing protein-tyrosine phosphatase 2 (SHP2) function drive selection of the recurrent Y62D and Y63C substitutions in Noonan syndrome. J Biol Chem 287(32): 27066-77.

Pettersen EF, Goddard TD, Huang CC, Couch GS, Greenblatt DM, Meng EC, Ferrin TE. 2004. UCSF Chimera--a visualization system for exploratory research and analysis. J Comput Chem 25(13): 1605-12.

Ren L, Chen X, Luechapanichkul R, Selner NG, Meyer TM, Wavreille AS, Chan R, Iorio C, Zhou X, Neel BG, Pei D. 2011. Substrate specificity of protein tyrosine phosphatases 1B, RPTPα, SHP-1, and SHP-2. Biochemistry 50(12): 2339-56.

Richards S, Aziz N, Bale S, Bick D, Das S, Gastier-Foster J, Grody WW, Hegde M, Lyon E, Spector E, Voelkerding K, Rehm HL; ACMG Laboratory Quality Assurance

Committee. 2015. Standards and guidelines for the interpretation of sequencevariants: a joint consensusrecommendation of the American College of Medical Genetics and Genomics and the Association for Molecular Pathology. Genet Med 17:405-424.

Roberts AE, Allanson JE, Tartaglia M, Gelb BD. 2013. Noonan syndrome. Lancet 381(9863): 333-42.

Sarkozy A, Carta C, Moretti S, Zampino G, Digilio MC, Pantaleoni F, Scioletti AP, Esposito G, Cordeddu V, Lepri F, Petrangeli V, Dentici ML, et al. 2009. Germline BRAF mutations in Noonan, LEOPARD, and cardiofaciocutaneous syndromes: molecular diversity and associated phenotypic spectrum. Hum Mutat 30:695-702.

Strullu M, Caye A, Lachenaud J, Cassinat B, Gazal S, Fenneteau O, Pouvreau N, Pereira S, Baumann C, Contet A, Sirvent N, Méchinaud F, et al. 2014. Juvenile myelomonocytic leukaemia and Noonan syndrome. J Med Genet 51(10): 689-97.

Sun H, Tan LP, Gao L, Yao SQ. 2009. High-throughput screening of catalytically inactive mutants of protein tyrosine phosphatases (PTPs) in a phosphopeptide microarray. Chem Commun (Camb) (6): 677-9.

Tajan M, de Rocca Serra A, Valet P, Edouard T, Yart A. 2015. SHP2 sails from physiology to pathology. Eur J Med Genet 58(10): 509-25.

Tartaglia M, Mehler EL, Goldberg R, Zampino G, Brunner HG, Kremer H, Van der Burgt I, Crosby AH, Ion A, Jeffery S, Kalidas K, Patton MA, et al. 2001. Mutations in PTPN11, encoding the protein tyrosine phosphatase SHP-2, cause Noonan syndrome. Nat Genet 29(4): 465-8.

Tartaglia M, Kalidas K, Shaw A, Song X, Musat DL, van der Burgt I, Brunner HG, Bertola DR, Crosby A, Ion A, Kucherlapati RS, Jeffery S, et al. 2002. PTPN11 mutations in Noonan syndrome: molecular spectrum, genotype-phenotype correlation, and phenotypic heterogeneity. Am J Hum Genet 70(6): 1555-63.

Tartaglia M, Niemeyer CM, Fragale A, Song X, Buechner J, Jung A, Hählen K, Hasle H, Licht JD, Gelb BD. 2003. Somatic mutations in PTPN11 in juvenile myelomonocytic leukemia, myelodysplastic syndromes and acute myeloid leukemia. Nat Genet 34(2): 148-50.

Tartaglia M, Niemeyer CM, Shannon KM, Loh ML. SHP-2 and myeloid malignancies. 2004a. Curr Opin Hematol 11(1):44-50

Tartaglia M, Martinelli S, Cazzaniga G, Cordeddu V, Iavarone I, Spinelli M, Palmi C, Carta C, Pession A, Aricò M, Masera G, Basso G, et al. 2004b. Genetic evidence for lineage-related and differentiation stage-related contribution of somatic PTPN11 mutations to leukemogenesis in childhood acute leukemia. Blood 104(2):307-13.

Tartaglia M, Martinelli S, Stella L, Bocchinfuso G, Flex E, Cordeddu V, Zampino G, Van der Burgt I, Palleschi A, Petrucci TC, Sorcini M, Schoch C, et al. 2006. Diversity and functional consequences of germline and somatic PTPN11 mutations in human disease. Am J Hum Genet 78(2): 279-90.

Tartaglia M, Gelb BD, Zenker M. 2011. Noonan syndrome and clinically related disorders. Best Pract Res Clin Endocrinol Metab 25(1): 161-79.

Wang W, Liu L, Song X, Mo Y, Komma C, Bellamy H, Zhao ZJ, Zhou GW. 2011. Crystal structure of human proteintyrosinephosphatase SHP-1 in the open conformation. J Cell Biochem 112(8): 2062-71.

Figure Legends

Figure 1. Structural characterization of SHP2 mutants. (A) Scheme of the SHP2 domain structure showing position of the residues affected by the newly identified *PTPN11* mutation cluster. (B) Ribbon representation of the three-dimensional structure of SHP2 in its autoinhibited conformation (PDB code 2SHP), following modeling of the loops missing in the crystallographic structure and energy minimization [Bocchinfuso et al., 2007]. The N-SH2, C-SH2 and PTP domains are colored in cyan, orange and pink, respectively. The Q loop motif (residues 505-513) is colored in red, while residues Leu^{261}, Leu^{262} and Arg^{265} are in dark green, blue and yellow, respectively. Helices B (residues 247-261) and C (residues 265-269) are indicated. (C) Interdomain interactions of Leu^{262}. The Leu^{262} side chain and the N-SH2 domain are reported as blue and cyan solid surface, respectively. Under the surface, residues Ala^{75}, Glu^{76} and Gln^{79} are shown as sticks. Substitutions at this codon are predicted to weaken the binding network between the N-SH2 and PTP domains stabilizing the inactive conformation of SHP2. (D) Interdomain interactions of Arg^{265}. The salt bridge involving Arg^{265} and Glu^{76} is highlighted as a dashed black line, with their side chains reported as sticks. Substitutions at this codon are predicted to weaken the binding network between the N-SH2 and PTP domains. (E) Region surrounding Leu^{261}. The side chain of Leu^{261} is reported as a dark green solid surface. The side chains of residues with atoms at less than 3.5 Å from Leu^{261} (*i.e.*, Gln^{257}, Glu^{258}, Lys^{260}, Tyr^{263}, Phe^{285}, Gln^{495}, and Arg^{498}) are reported as semi-transparent gray surfaces, under which atoms are shown in sticks representation. Substitutions affecting this residue are predicted to perturb the hydrophobic binding network stabilizing this region of the PTP domain.

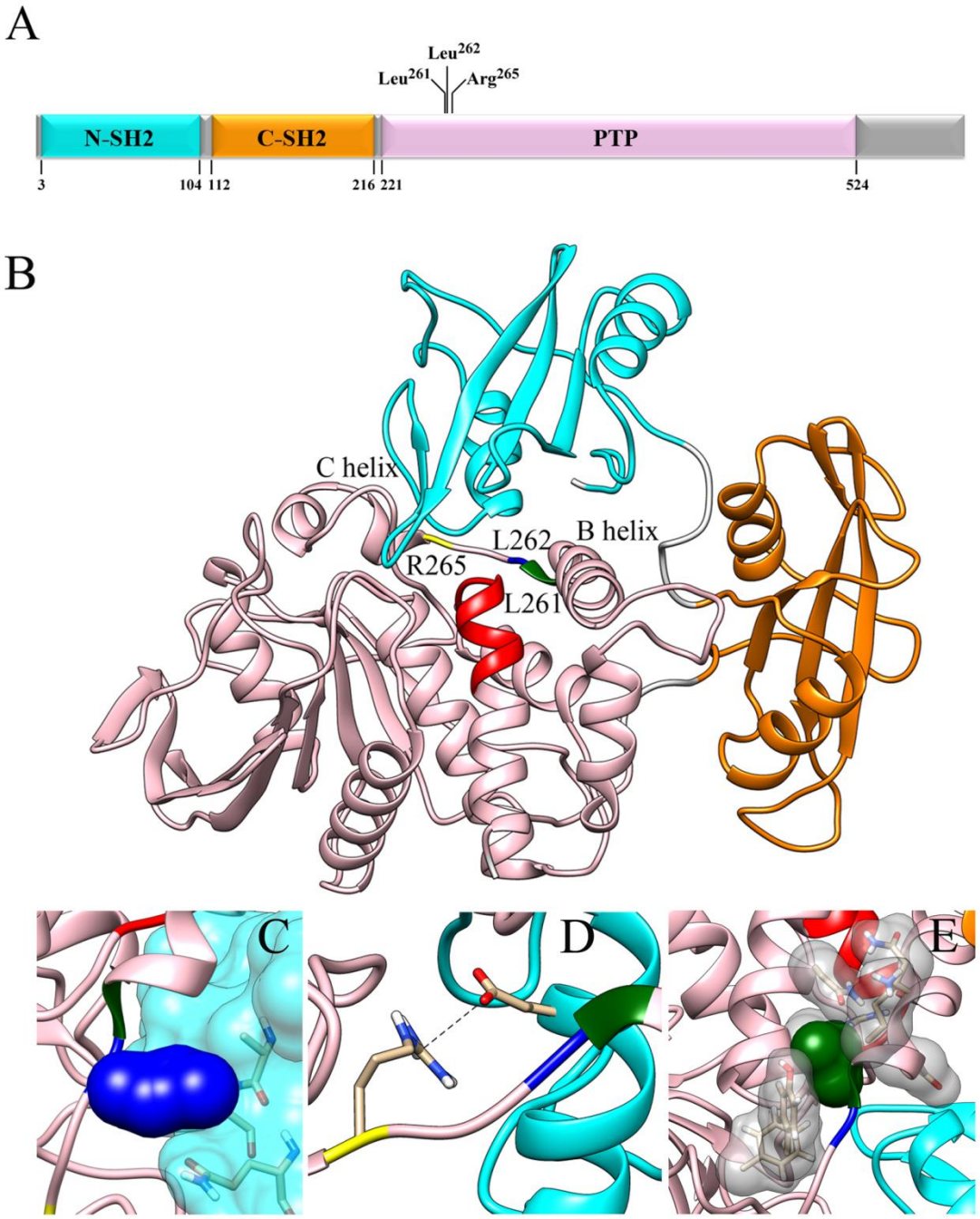

Figure 2. Molecular dynamics simulations. Surfaces of the PTP structure of $SHP2^{WT}$ (A), $SHP2^{L261H}$ (B) and $SHP2^{L261F}$ (C) resulting after 100 ns of simulation and removal of the SH2 domains. Surfaces are colored as a function of the Root Mean Square Fluctuations (RMSF) calculated from last 50 ns of the MD simulations. Blue and red indicate regions with lower and higher fluctuations, respectively. For comparison, the protein backbone is also reported (D). The color code is the same as in Fig. 1, except for the Q loop motif (see below). Residues belonging to the pY loop (residues 273-279 and 282), WPD loop (420 and 423-429), PTP loop (454-467), and Q loop motif (505-513), with an established role in the catalysis, are colored in dark gray.

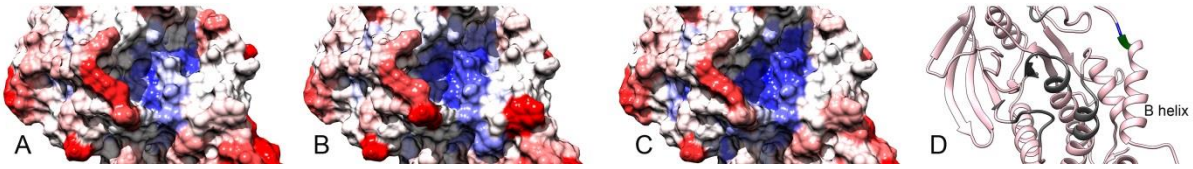

Figure 3. ERK phosphorylation assays. Newly identified NS-causing mutations promote variably enhanced ERK phosphorylation. Representative blots (above) and mean ± SD densitometry values (below) of three independent experiments are shown. HEK293T cells were co-transfected with FLAG-tagged Gab1 and the indicated V5-tagged SHP2 constructs. Following transfection, cells were serum-starved and treated with 30 ng/ml EGF for 5 or 15 minutes, or left unstimulated. Equal amounts of cell lysates were resolved on 10% polyacrylamide gel. Membranes were probed with anti-phosphoERK1/2 antibody. Aliquots of corresponding cell lysates were probed with anti-ERK1/2, anti-V5 and anti-FLAG antibodies. Asterisks indicate significant differences compared with wild-type SHP2 at the corresponding time upon EGF stimulation (**P*<0.05; ***P*<0.002; Student's *t*-test).

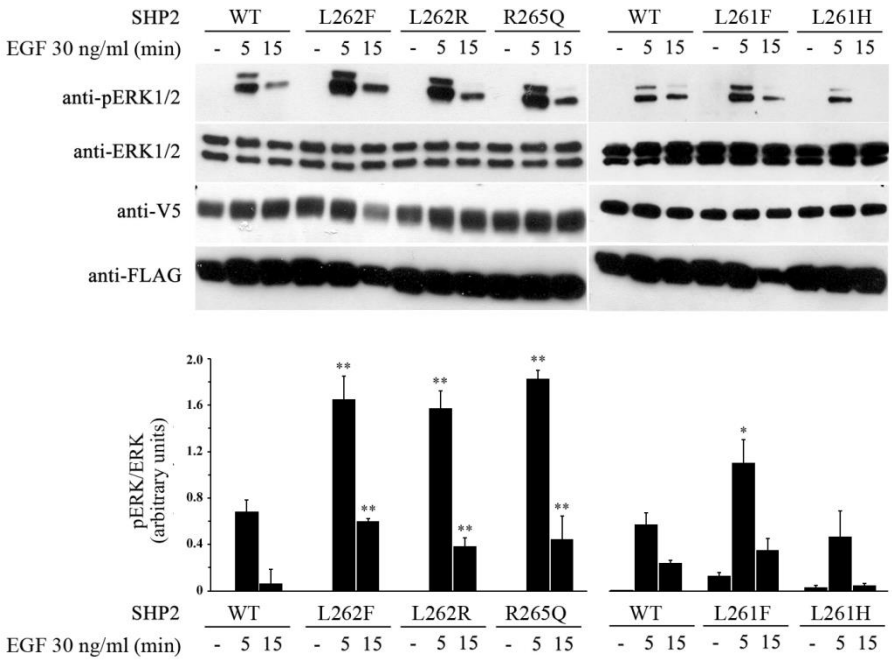

Figure 4. Phosphatase assays. (A) *In vitro* phosphatase assay of wild-type and mutant SHP2 proteins. The leukemia-associated p.A72V change is shown for comparison. Catalytic activity was measured as pmoles of phosphate released using pNPP as a substrate, basally (white bars) and following stimulation with 10 μM BTAM peptide (black bars). Asterisks indicate significant differences compared with wild-type SHP2 (**P*<0.01; ***P*<0.001; Student's *t*-test). (B) Phosphatase assay of SHP2 proteins as a function of BTAM peptide concentration. Note the enhanced catalytic activation of the $SHP2^{L261H}$ and $SHP2^{L261F}$ proteins at high BTAM peptide concentration, compared with wild-type SHP2. (C) Activities of the recombinant wild-type and mutant (p.L261F and p.L261H) isolated PTP domains of SHP2 ($SHP2_{PTP}$). (D) Change in substrate selectivity of $SHP2_{PTP}^{L261F}$ and $SHP2_{PTP}^{L261H}$ proteins evaluated by malachite green assay, using the $GAB1_{Y657}$, $p190A/RhoGAP_{Y1105}$ and $EGFR_{Y1016}$ phosphopeptides as substrates. Asterisks indicate significant differences compared with wild-type SHP2 (**P*<0.05).

In all assays, absorbance values are expressed as mean ± SD of at least three independent experiments, and are normalized to the basal activity of the wild-type enzyme.

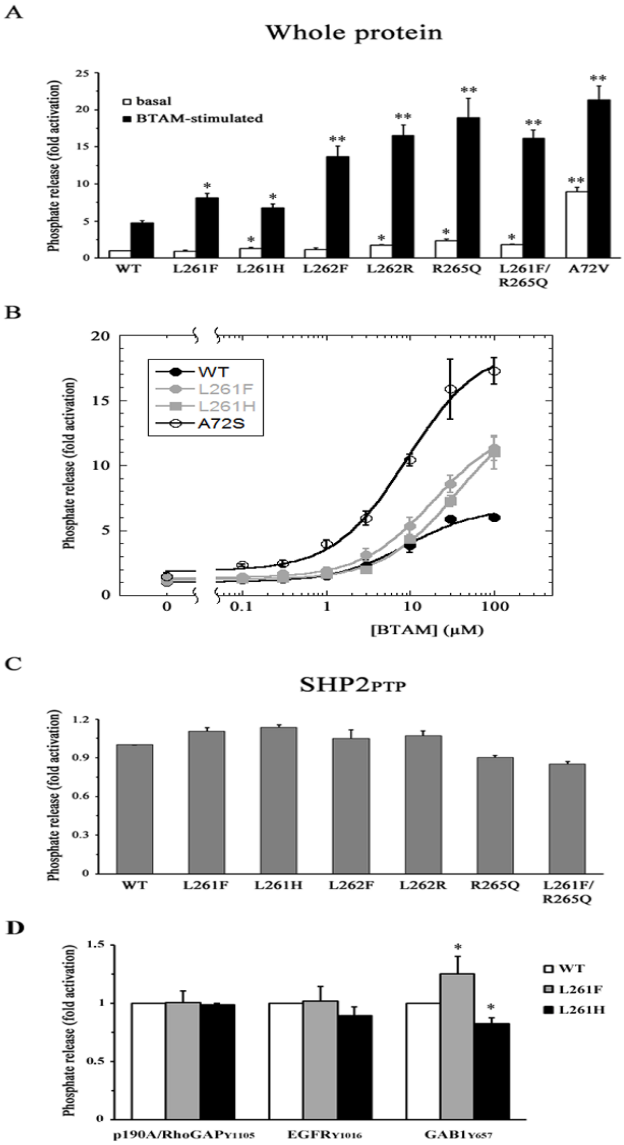

Table 1. *PTPN11* missense changes specifying a novel mutation cluster underlying NS.

Exon	Nucleotide Change	ExAC allele frequency	Amino acid Change	Domain	Number of unrelated cases	Origin	MetaSVM[a]	CADD phred[a]	REVEL[a]	ACMG
7	c.781C>T	-	p.L261F	PTP	6[b]	4 *de novo*, 2 familial	0.98	24.6	0.547	pathogenic
7	c.782T>A	0.0000084	p.L261H	PTP	1	familial	0.91	24.5	0.558	unknown significance[c]
7	c.784C>T	-	p.L262F	PTP	1	familial	1.10	23.3	0.529	pathogenic
7	c.785T>G	-	p.L262R	PTP	3	2 *de novo*, 1 familial	1.12	25.4	0.708	pathogenic
7	c.794G>A	0.000042	p.R265Q	PTP	6[b]	2 *de novo*, 4 familial	1.10	27.4	0.814	pathogenic

Nucleotide numbering reflects cDNA numbering with 1 corresponding to the A of the ATG translation initiation codon in the *PTPN11* reference sequence (NM_002834.3).

[a]Scores >0 (MetaSVM), >15 (CADDphred) or >0.5 (REVEL) predict a significant impact of the sequence change on protein structure and function.

[b]Including one case with co-occurrence of L261F and R265Q substitutions in *cis*.

[c]While there are experimental data indicating that this variant perturbs SHP2's function and MAPK signaling and is believed to have a mild clinical impact, in the absence of additional evidence supporting pathogenicity, this change is formally classified as a variant of unknown significance.

This article has been accepted for publication and undergone full peer review but has not been through the copyediting, typesetting, pagination and proofreading process, which may lead to differences between this version and the Version of Record. Please cite this article as doi: 10.1002/humu.23175.